Process–Structure–Property Relationship in Ternary Short-Glass-Fiber/Elastomer/Polypropylene Composites

S. C. Tjong,[1] S. A. Xu,[1] Y. W. Mai[2,3]

[1]*Department of Physics and Materials Science, City University of Hong Kong, Tat Chee Avenue, Kowloon, Hong Kong*
[2]*Center for Advanced Materials Technology, University of Sydney, Sydney, NSW 2006, Australia*
[3]*Department of Manufacturing Engineering and Engineering Management, City University of Hong Kong, Tat Chee Avenue, Kowloon, Hong Kong*

Received 9 April 2002; accepted 13 July 2002
Published online 19 February 2003 in Wiley InterScience (www.interscience.wiley.com). DOI 10.1002/app.11777

ABSTRACT: Short-glass-fiber (SGF)-reinforced polypropylene (PP) composites toughened with a styrene/ethylene butylene/styrene (SEBS) triblock copolymer were injection molded after extrusion. Furthermore, a maleic anhydride (MA)-grafted SEBS copolymer (SEBS-*g*-MA) was used as an impact modifier and compatibilizer. The effects of the processing conditions and compatibilizer on the microstructure and tensile and impact performance of the hybrid composites were investigated. In the route 1 fabrication process, SGF, PP, and SEBS were blended in an extruder twice, and this was followed by injection molding. In route 2, or the sequential blending process, the elastomer and PP were mixed thoroughly before the addition of SGF. In other words, either PP and SEBS or PP and SEBS-*g*-MA pellets were premixed in an extruder. The produced pellets were then blended with SGF in the extruder, and this was followed by injection molding. The SGF/SEBS-*g*-MA/PP hybrid fabricated by the route 2 process exhibited the highest modulus, yield stress, tensile stress at break, Izod impact energy, and Charpy drop weight impact strength among the composites investigated. This was due to the formation of a homogeneous SEBS elastomeric interlayer at the SGF and matrix interface of the SGF/SEBS-*g*-MA/PP hybrid. This SEBS rubbery layer enhanced the interfacial bonding between SGF and the matrix of the SGF/SEBS-*g*-MA/PP hybrid. The correlations between the processing, microstructure, and properties of the hybrids were investigated. © 2003 Wiley Periodicals, Inc. J Appl Polym Sci 88: 1384–1392, 2003

Key words: compatibility; composites; compounding; elastomers; mechanical properties

INTRODUCTION

Polypropylene (PP) is a versatile commodity thermoplastic with a wide range of domestic and industrial applications because of its good processability and relatively low cost. PP is also commonly used as a matrix material for polymer composites. Despite its extensive potential applications, PP exhibits poor impact strength at low temperatures. To overcome this drawback, PP is usually blended with elastomeric particles, such as styrene/ethylene butylene/styrene triblock copolymer (SEBS), ethylene–propylene rubber (EPR), and ethylene–propylene–diene monomer. Generally, the incorporation of SEBS into PP leads to a substantial reduction in its yield strength and stiffness.[1–4] To maintain a stiffness-to-toughness balance, inorganic reinforcements such as glass beads (GBs) and fillers are incorporated into the PP/SEBS blends, and this leads to the formation of hybrid composites.[5,6] Recently, particular attention has been paid to the fabrication and mechanical properties of short-fiber-reinforced PP composites toughened with elastomers.[7,8] For example, Jancar[6] studied the effect of the elastomer content on the yielding and impact behavior of maleated short-glass-fiber (SGF)/PP/EPR blends. The results showed that the Charpy notched impact strength of composites at −20°C tends to increase with an increasing volume of EPR. Large plastic deformation in the fiber–matrix interface and fiber pullout are the primary energy dissipative processes during yielding and impact fracture.[7] Tam et al.[7] also indicated that fiber debonding and pullout are the main energy absorption mechanisms for SGF/EPR/PP hybrids. The elastomers have hardly any toughening effect on the hybrids.[7] Little information is available in the literature concerning the fracture properties of SEBS-toughened PP hybrids containing short-fiber reinforcements. More recently, Wu et al.[8] reported that the SEBS interface layer formed at the wood fiber/matrix region is beneficial for improving the impact toughness of PP hybrids. This is because the SEBS layer can release the plastic constraint from the rigid fibers during impact testing, thereby inducing massive plastic deformation in the PP matrix.[9]

Correspondence to: S. C. Tjong (aptjong@cityu.edu.hk).
Contract grant sponsor: Research Grants Council of Hong Kong Special Administrative Region, China; contract grant number: CityU 1029/00E.

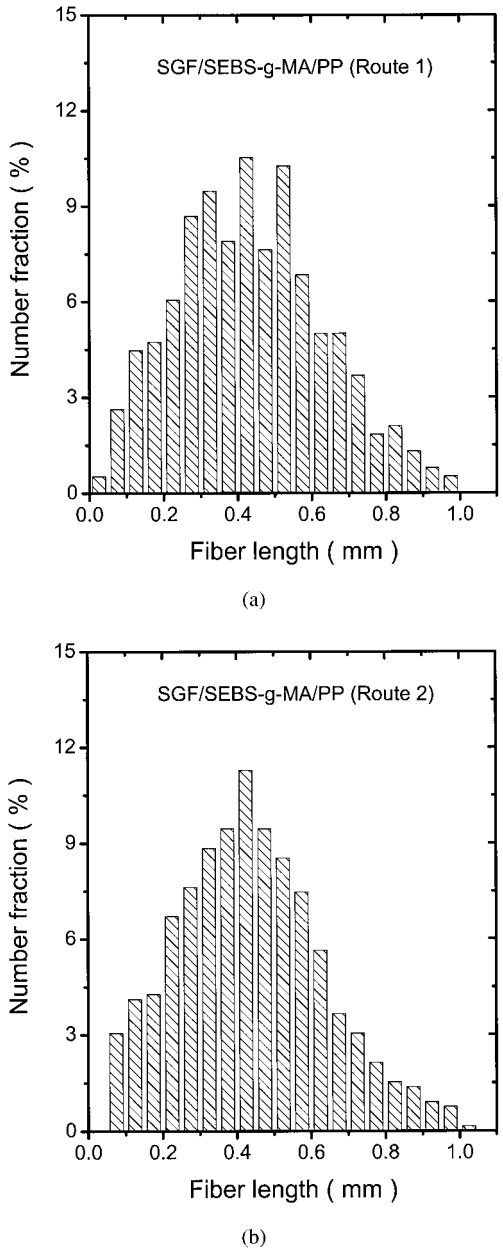

Figure 1 Number fraction versus the fiber length distribution of (a) SGF/SEBS-*g*-MA/PP (route 1) and (b) SGF/SEBS-*g*-MA/PP (route 2) hybrids.

It is generally accepted that the processing conditions have a strong influence on the resulting structures of short-fiber-reinforced composites. Microstructure-related parameters, such as the types of matrices, the types and volume fractions of fibers, the fiber length distributions and orientations, and the fiber–matrix interfaces, can affect the mechanical performances of composites.[10,11] Furthermore, the addition of appropriate compatibilizers during the processing of composites is known to improve their mechanical performance. This improvement is attributed to an increase in adhesion between the fibers and matrices of composites, which allows more efficient stress transfer across the fiber–matrix interface. For SGF-reinforced SEBS/PP hybrids, maleic anhydride (MA)-grafted SEBS (SEBS-*g*-MA) can act as a compatibilizer for the composites. However, little information is available on their processing–structure–property relationships. In a previous study, we carried out a preliminary investigation of fabrication on SGF/maleated SEBS/PP hybrid composites.[12] The hybrid was prepared by extrusion and subsequent injection molding. The results showed that maleated SEBS (SEBS-*g*-MA) improved the yield strength and impact toughness of the hybrid composites. Extensive plastic deformation occurred at the matrix interface layer next to the fibers of the SGF/SEBS-*g*-MA/PP composites during impact testing. This was due to the MA functional group grafted to SEBS, which enhanced the adhesion between SEBS and SGF.[12] This study investigated the processing–structure–property relationships of SGF/SEBS/PP and SGF/SEBS-*g*-MA/PP hybrids.

EXPERIMENTAL

Materials

The materials used in this study were PP homopolymer (Profax 6331, Himont Co.), SEBS (Kraton G6151, Shell Co.), SEBS-*g*-MA (Kraton FG 1901X, Shell, Houston, TX), and SGF (ca. 4 mm long; 144A-14C, Owens Corning). The glass fiber was not treated with a coupling agent.

Blending

All the materials used were dried separately in ovens for more than 48 h. Two melt mixing routes were used to prepare the SGF/SEBS/PP and SGF/SEBS-*g*-MA/PP hybrids. The weight ratio of SGF, SEBS or maleated SEBS, and PP was fixed at 23.1:15.4:61.5. In the route 1 process, dried elastomer and PP pellets, as well as SGF, were initially mixed in a Brabender twin-screw extruder (Germany) with an operating temperature profile of 180–190–220–220°C. The extrudates were pelletized and mixed again in a Brabender extruder under the same conditions. Then, the extruded strands were chopped into granules. In the route 2 process, either SEBS and PP or SEBS-*g*-MA and PP pellets at a 20:80 weight ratio were initially mixed in a Brabender extruder, and the blend extrudates were granulized. The heating zones of the extruder were also set at 180–190–220–220°C. The resulting pellets and SGF were then compounded with the same extruder under the same processing conditions. The extrudates were pelletized into granules. Route 2 is known as a sequential compounding process: the elastomer and PP were mixed thoroughly before the addition of SGF. Finally, the pellets obtained either by route 1 or route 2 were dried in an oven at 100°C for

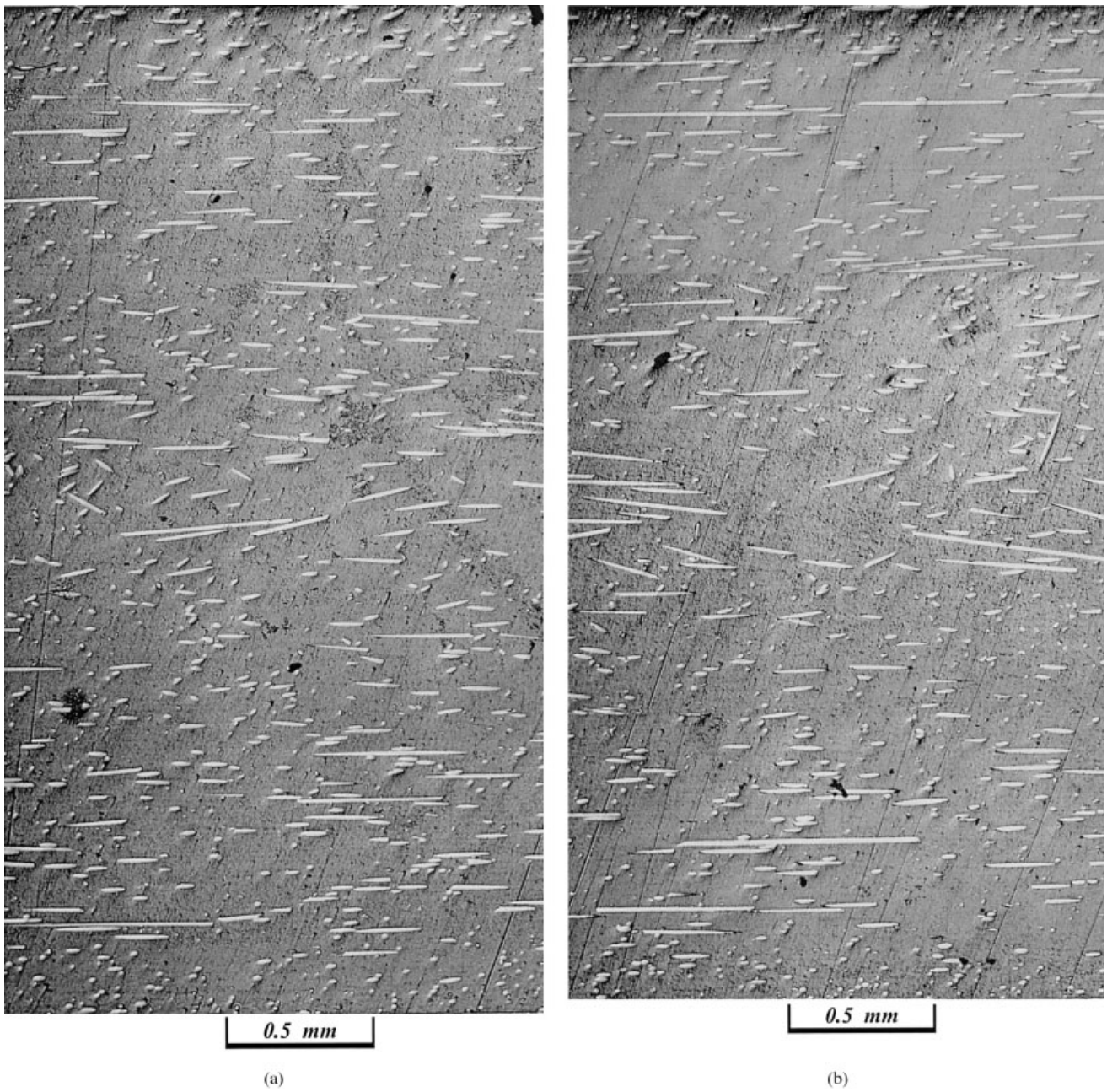

Figure 2 Cross-sectional optical micrographs of (a) SGF/SEBS-*g*-MA/PP (route 1) and (b) SGF/SEBS-*g*-MA/PP (route 2) hybrids (view along the MFD).

48 h. The dried pellets were fed into an injection molder to produce standard tensile bars (ASTM D 638-91) and plaques (200 mm × 80 mm × 3.2 mm).

Fiber distribution and orientation

Small hybrid composites were cut from the injection-molded plaques and burned in a muffle furnace. The remaining fibers were collected, ultrasonically cleaned in acetone, and viewed under an image analyzer for the determination of the fiber length distribution [Fig. 1(a,b)]. The SGF length was reduced to less than 1 mm by the blending and injection-molding processes, as expected. From the distribution diagrams, there was a strong number fraction of fibers with a length between 0.3 and 0.5 mm after processing.

Morphology observation

Samples approximately 10 mm long were cut from the midsections of tensile bars and subsequently fractured in liquid nitrogen along the injection-molding direction. The cryofractured samples were etched in a tetrahydrofuran (THF) solvent for 6 h so that the elasto-

meric particles from the matrix would be dissolved. They were then washed with fresh THF and dried in an oven operated at 40°C. Finally, the surfaces were coated with a thin layer of gold before examination with a scanning electron microscope (JEOL JSM 820). For the optical microscopy examination, samples were cut from the plaques, polished, and observed with an optical microscope.

Mechanical characterization

The static tensile behavior of the samples was determined at 21°C with an Instron tester (model 4206) at a crosshead speed of 10 mm/min. Five specimens of each composition were tested, and the average value was reported.

Izod notched impact samples were cut from the injection-molded plaques with the longitudinal direction of the specimens parallel to the mold filling direction (MFD). Izod impact measurements were carried out with a Ceast pendulum impact tester (Italy) at 21°C. Moreover, standard V-notched Charpy drop weight impact specimens (125 mm × 13 mm × 3.2 mm) were cut from the injection-molded plaques. The longitudinal direction of the Charpy impact specimens also aligned along the MFD. A Ceast Fractovise drop weight system was used to conduct instrumented Charpy impact tests. The system was equipped with

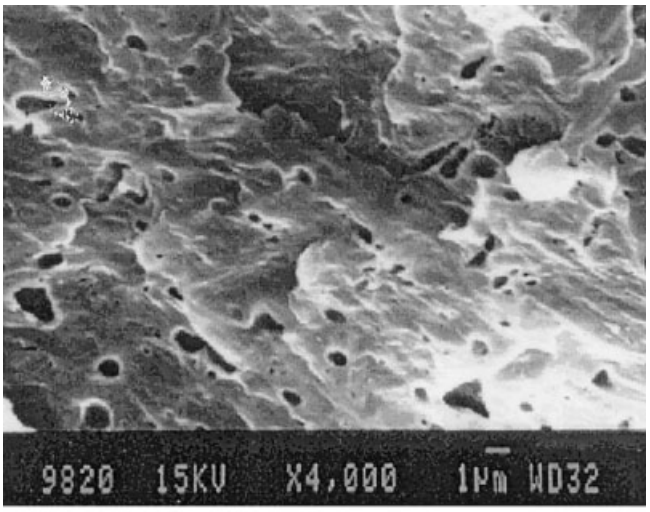

(a)

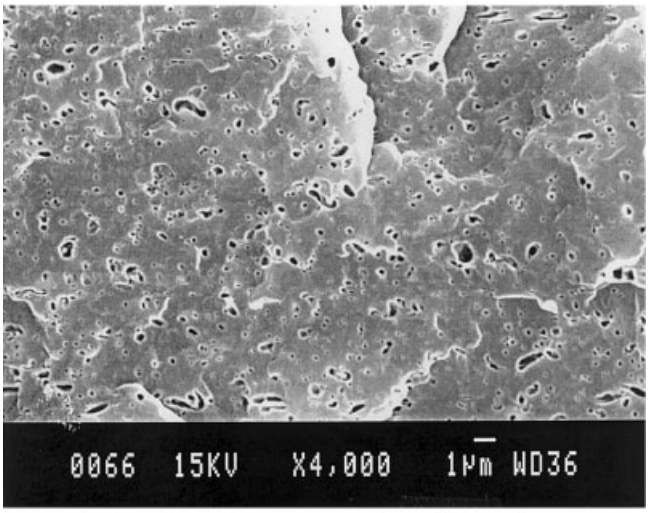

(b)

Figure 3 SEM micrographs showing the dispersion of SEBS particles in the matrices of SGF/SEBS/PP hybrids prepared by (a) route 1 and (b) route 2 processes. The SEBS particles were extracted by the immersion of the hybrids in THF solutions.

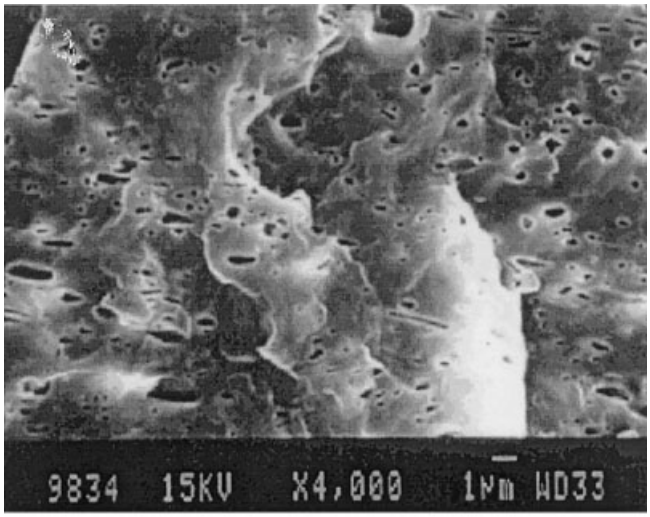

(a)

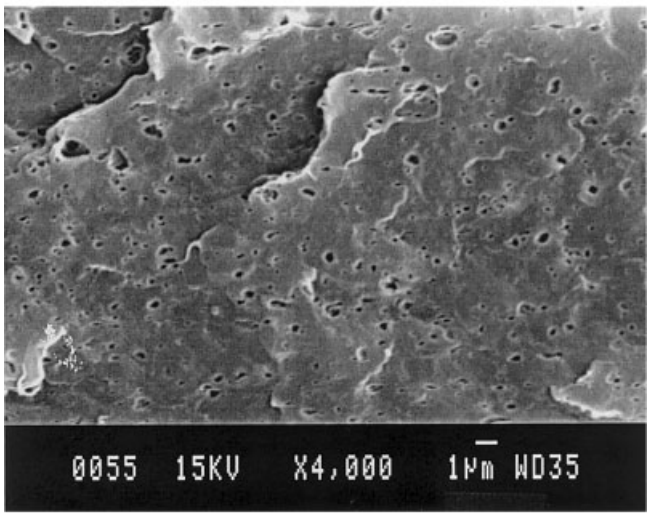

(b)

Figure 4 SEM micrographs showing the dispersion of SEBS particles in the matrices of SGF/SEBS-*g*-MA/PP hybrids prepared by (a) route 1 and (b) route 2 processes. The SEBS particles were extracted by the immersion of the hybrids in THF solutions.

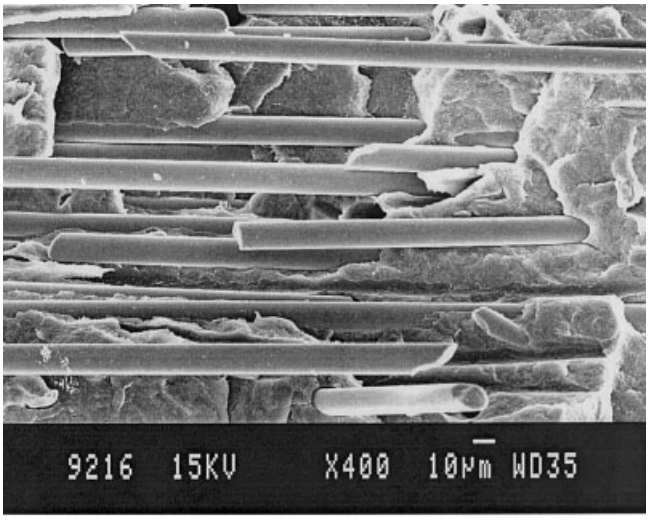

(a)

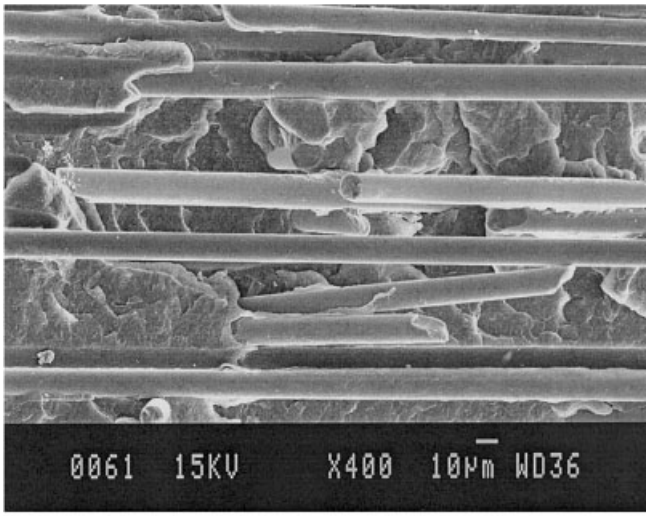

(b)

Figure 5 SEM micrographs showing the cryofracture surface morphology of SGF/SEBS/PP hybrids prepared by (a) route 1 and (b) route 2 processes.

an instrumental tup, and the signal was fed to a spectrum analyzer. Load–time curves were obtained by computerized data acquisition. The mass of a striker was 3.164 kg, and the span of a sample support was 95.3 mm. The impact speeds varied from 0.75 to 5 m s^{-1}, and the free clearance (drop height) ranged from 0.0287 m to 1.275 m accordingly. Five specimens were tested at each speed, and the average value was reported. The fracture surfaces of the impact specimens were examined with scanning electron spectroscopy (SEM).

Dynamic mechanical analysis (DMA)

Samples (60 mm × 13 mm × 3.2 mm) for DMA were also cut from the injection-molded plaques with the axis parallel to the MFD. The measurements were conducted with a TA Instruments model DMA 2980 (New Castle, DE) at a rate of 5°C min^{-1}. The temperature of the test ranged from −100 to 150°C. The frequency was 1 Hz, and the oscillation amplitude was 0.3 mm.

RESULTS AND DISCUSSION

Morphology

Figure 2(a,b) presents cross-sectional optical micrographs showing the fiber orientation in the hybrids. A skin–core structure can be observed; that is, the fibers aligned preferentially along the MFD in the skin layer but aligned randomly in the core region. Figures 3(a,b) and 4(a,b) present SEM micrographs showing the dis-

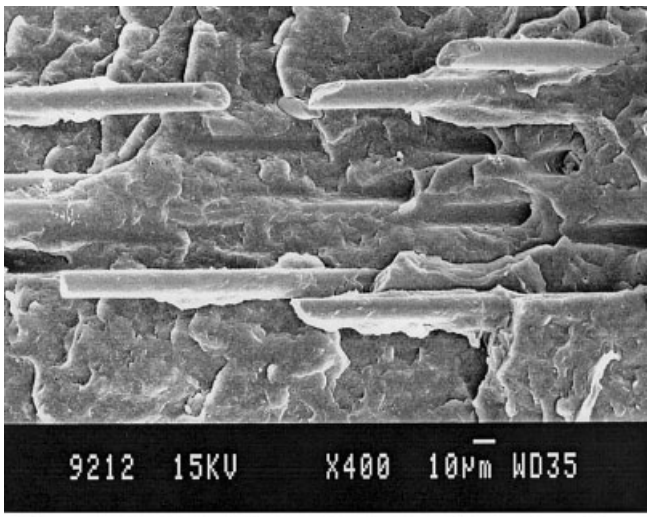

(a)

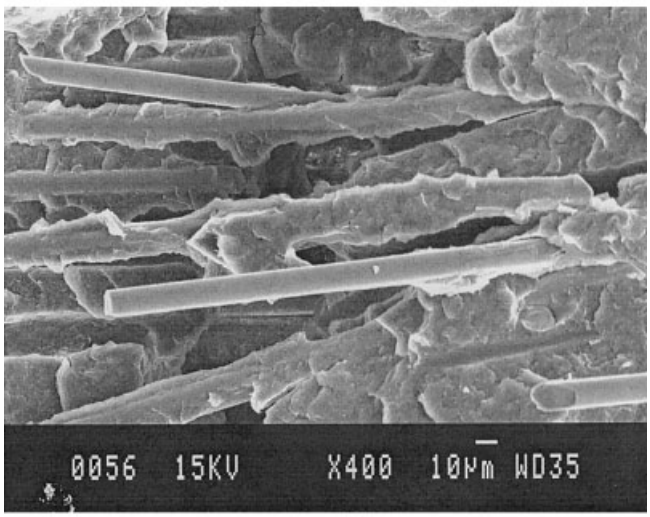

(b)

Figure 6 SEM micrographs showing the cryofracture surface morphology of SGF/SEBS-*g*-MA/PP hybrids prepared by (a) route 1 and (b) route 2 processes.

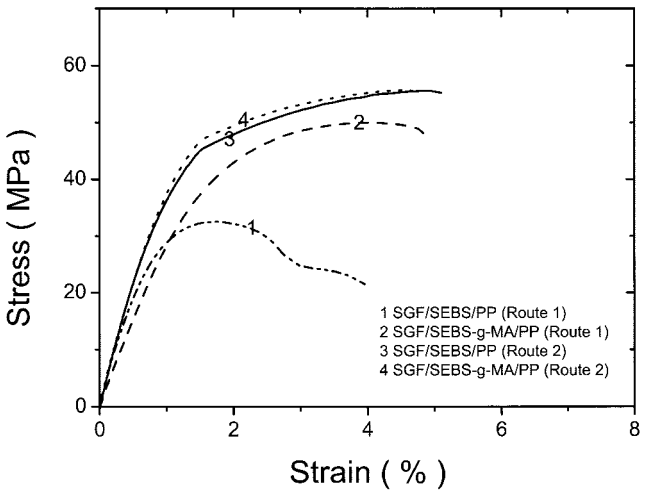

Figure 7 Stress–strain curves of SGF/SEBS/PP and SGF/SEBS-*g*-MA/PP hybrids prepared by both processing routes.

persion of SEBS particles in the matrices of SGF/SEBS/PP and SGF/SEBS-*g*-MA/PP hybrids fabricated by routes 1 and 2, respectively. The samples were etched in THF solutions before the SEM observations. The small voids observed in these micrographs were derived from SEBS because the elastomeric particles dissolved in the THF solutions during etching. These micrographs reveal that the size of SEBS of the hybrids prepared by route 2 was finer and more homogeneous than that of composites fabricated by the route 1 process.

Figure 5(a,b) presents SEM micrographs showing the morphology of cryofracture surfaces of SGF/SEBS/PP hybrid prepared by routes 1 and 2, respectively. The fiber surfaces of the SGF/SEBS/PP composites prepared by both processes were relatively clean. This implies that the interfacial adhesion between SGF and the matrix was quite poor. In contrast, the fiber surfaces of the SGF/SEBS-*g*-MA/PP composite specimens fabricated by both routes were coated with the matrix material, and this indicated that a strong bonding developed between SGF and SEBS [Fig. 6(a,b)]. This bonding was due to the fact that the MA functional groups grafted to the ethylene butylene (EB) midblock of SEBS could react with hydroxyl groups on the SGF surfaces during compounding. The reaction between SEBS-*g*-MA and SGF can be depicted as follows:

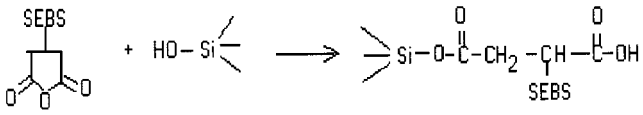

Recently, Karger-Kocsis et al.[12] and Stricker et al.[5] reported that the SEBS elastomer tends to encapsulate the GB surfaces of GB/SEBS-*g*-MA/PP hybrids, and this leads to the formation of a core–shell structure. In other words, an elastomeric SEBS interlayer is formed between the GBs and the PP matrix. Such a layer enhances the interfacial adhesion and tensile yield stress.[5] For SGF/SEBS/PP and SGF/SEBS-*g*-MA/PP hybrids, several types of interfacial bonding could develop between the phase components of the hybrids. The interfacial bonding between SGF and SEBS is relatively poor, but it can be improved by the grafting of SEBS with MA functional groups, as previously discussed. The interaction between SGF and PP is limited because SGF exhibits a polar surface and PP is a nonpolar polyolefin. However, SEBS has good compatibility with PP because the EB midblock of SEBS can diffuse into the PP phase, forming small micelles. The interdiffusion between the EB block of SEBS and PP enhances the interfacial adhesion between SEBS and PP.[3] Taking the combination of good interfacial interactions between SEBS and SGF and between SEBS and PP into consideration, we see that a ductile SEBS layer could form at the SGF and PP matrix of SGF/SEBS-*g*-MA/PP hybrids. Indeed, SEM micrographs indicate that the fiber surfaces of the SGF/SEBS-*g*-MA/PP hybrid are coated with the matrix material (Fig. 6). This rubbery layer is thought to have a similar function to that formed in the GB/SEBS-*g*-MA/PP and wood fiber/SEBS-*g*-MA/PP hybrids.[8,9,12,13] As mentioned previously, route 2 (i.e., the sequential blending process) produces a finer and homogeneous dispersion of elastomer particles in the matrix of the SGF/SEBS-*g*-MA/PP hybrid. Therefore, the rubbery interlayer formed in the SGF/SEBS-*g*-MA/PP hybrid (route 2) is more homogeneous in thickness than that formed in this hybrid prepared by the route 1 process. This is because the route 2 process allows PP and SEBS-*g*-MA to be mixed thoroughly before the addition of SGF. However, this thin layer is unlikely to form at the fiber–PP matrix interface of the SGF/SEBS/PP hybrid samples fabricated by both routes.

TABLE I
Tensile Properties of the Hybrids

Sample	Modulus (MPa)	Yield stress (MPa)	Stress at break (MPa)	Elongation (%)
SGF/SEBS/PP (route 1)	4251 ± 164	33 ± 0.2	20 ± 0.2	3.9 ± 0.13
SGF/SEBS/PP (route 2)	4656 ± 176	54 ± 0.6	54 ± 0.4	5.1 ± 0.15
SGF/SEBS-*g*-MA/PP (route 1)	3346 ± 128	50 ± 0.5	49 ± 0.6	5.0 ± 0.17
SGF/SEBS-*g*-MA/PP (route 2)	4755 ± 189	54 ± 0.8	55 ± 0.8	4.8 ± 0.14

TABLE II
Notched Izod Impact Properties of the Hybrids

Sample	Impact strength (kJ/m^2)
SGF/SEBS/PP (route 1)	8.26 ± 0.51
SGF/SEBS/PP (route 2)	9.63 ± 0.65
SGF/SEBS-*g*-MA/PP (route 1)	9.70 ± 0.83
SGF/SEBS-*g*-MA/PP (route 2)	13.94 ± 1.05

Static tensile properties

Figure 7 shows the stress–strain curves for the SGF/SEBS/PP and SGF/SEBS-*g*-MA/PP hybrids prepared by both processing routes. The tensile properties of these hybrids are summarized in Table I. Apparently, the SGF/SEBS-*g*-MA/PP hybrid prepared by route 2 exhibited the highest modulus, yield stress, and tensile stress at break. This was due to the formation of a homogeneous SEBS interlayer that could promote efficient stress transfer from the matrix to SGF during the tensile loading process.

Izod and charpy impact properties

The notched Izod impact strengths of the SGF/SEBS/PP and SGF/SEBS-*g*-MA/PP hybrids fabricated by routes 1 and 2 are listed in Table II. Apparently, the impact strength of the SGF/SEBS-*g*-MA/PP hybrid fabricated by either route 1 or route 2 was considerably higher than that of the SGF/SEBS/PP composite prepared under similar conditions. As composite materials are often subjected to high impact loading rates during their service lives, the effects of the impact velocity on the performance of these hybrids must be determined. Figure 8 shows the variations of the notched Charpy impact strengths of the hybrids investigated with the impact velocity. The SGF/SEBS/PP composite fabricated by route 1 exhibited a higher impact strength than the SGF/SEBS-*g*-MA/PP hybrid (route 1) under impact velocities less than or equal to 2 m s^{-1}. Above 2 m s^{-1}, the impact energy of the SGF/SEBS-*g*-MA/PP hybrid (route 1) was slightly higher than that of its counterpart. For route 2 fabri-

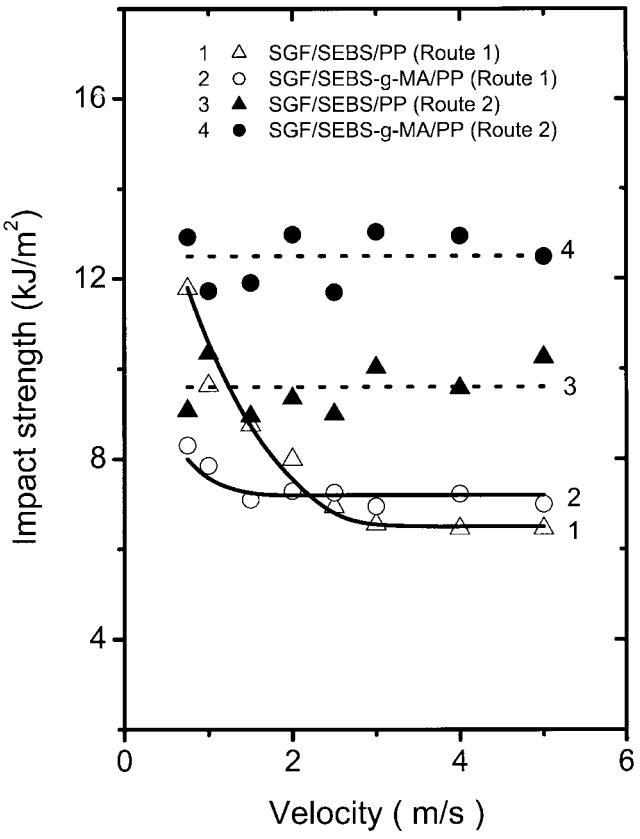

Figure 8 Notched Charpy impact strength of the hybrids investigated versus the impact velocity.

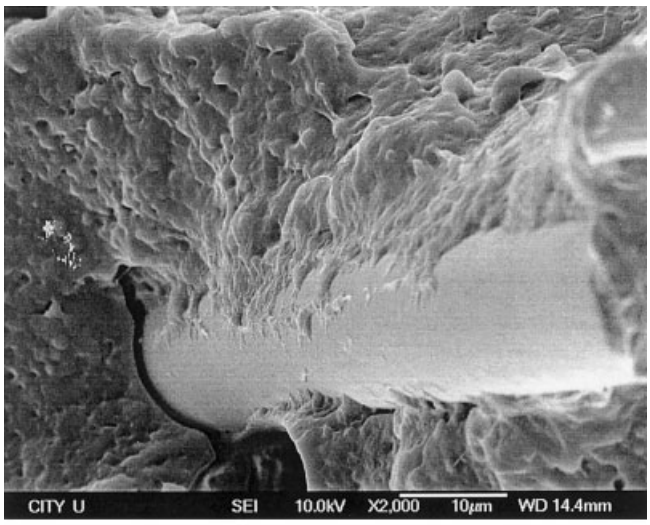

(a)

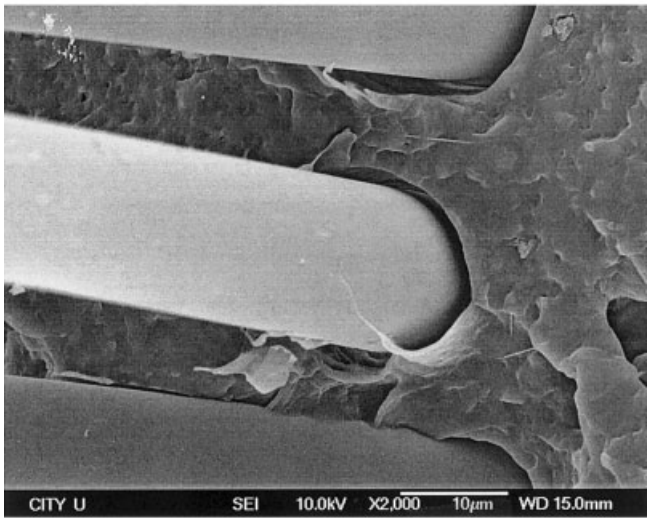

(b)

Figure 9 SEM fractographs of (a) SGF/SEBS-*g*-MA/PP (route 2) and (b) SGF/SEBS/PP (route 2) hybrids tested at an impact velocity of 3 m s^{-1}.

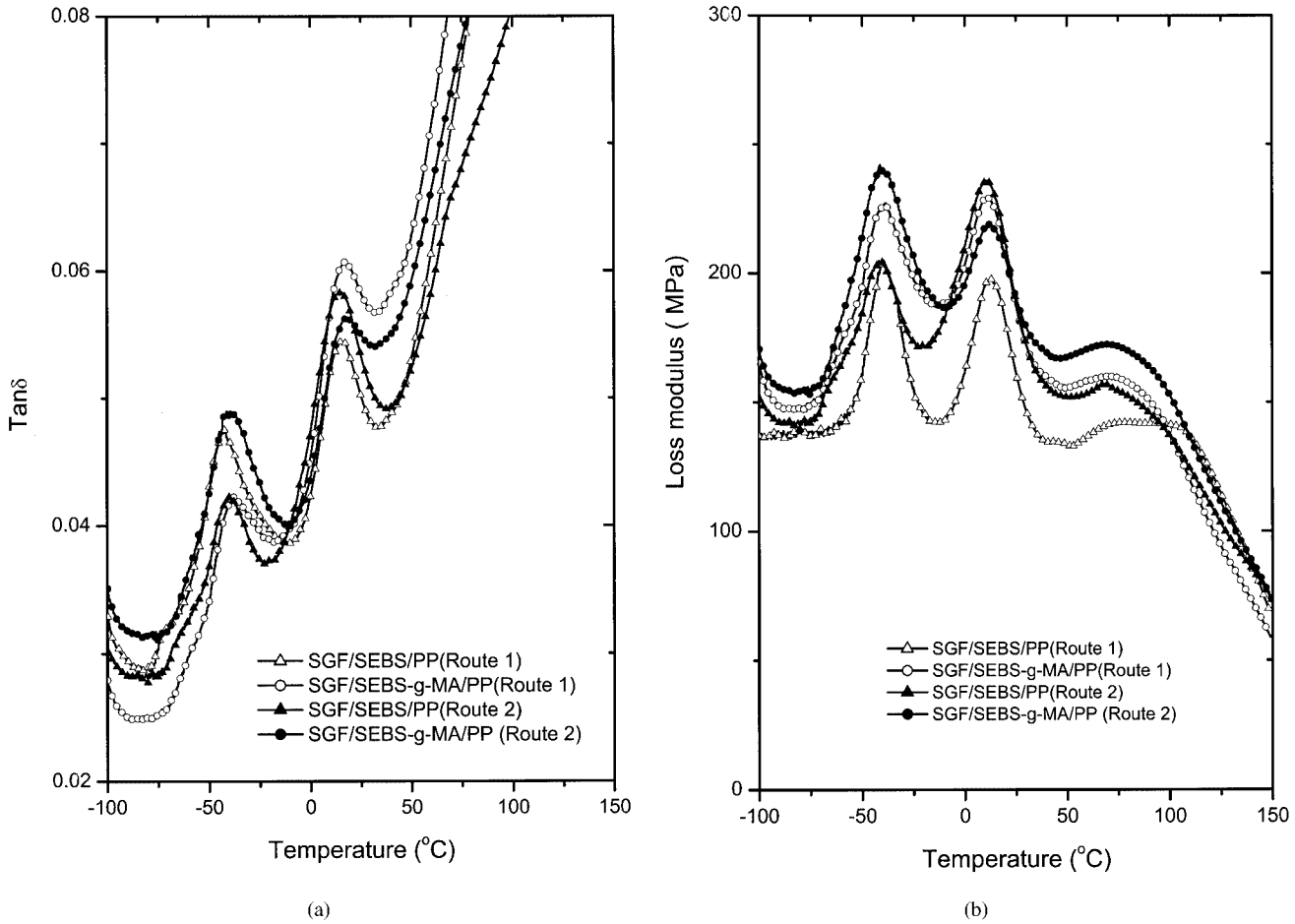

Figure 10 (a) Tan δ and (b) loss modulus profiles of the hybrids investigated as a function of temperature.

cation, the SGF/SEBS-*g*-MA/PP hybrid also exhibited a much higher impact strength than the SGF/SEBS/PP composite. The impact strengths of both hybrids prepared by route 2 were independent of the impact velocities.

Figure 9(a) shows SEM fractograph of the SGF/SEBS-*g*-MA/PP composite (route 2) tested at an impact velocity of 3 m s^{-1}. It is evident that the SGF surfaces were bonded with a thin layer of matrix material, that is, an SEBS interlayer. Extensive plastic deformation can be observed in the matrix region adjacent to the fiber ends [Fig. 9(a)]. Wu et al.[8] reported that the SEBS encapsulating layer is highly ductile and capable of relaxing laterally in response to the triaxial stress under impact loading. This interface may undergo debonding cavitation to relieve the triaxial stress imposed by the plane strain constraint at the notch tip. The relaxation of the interface can prevent premature brittle failure for the matrix and the fiber–matrix interface during impact loading. In this study, the SGF/SEBS-*g*-MA/PP hybrid (route 2) possessed the highest modulus, yield stress, tensile stress at break, Izod impact energy, and Charpy drop weight impact strength as well as a fine dispersion of SEBS elastomers in the PP matrix. These beneficial effects were contributed by the formation of a homogeneous SEBS thin layer at the fiber–matrix interface that enhanced interfacial adhesion. This layer enabled more efficient stress transfer across the fiber–matrix interface under tensile loading and relieved the triaxial stress imposed by the plane strain constraint at the notch tip during the impact test. Furthermore, the rubbery SEBS interlayer could deflect the propagation of cracks during impact loading. Such deflections not only dissipated a large amount of the fracture energy but also prevented brittle failure for the SGF and SGF–matrix interface. In contrast, the SGF surfaces of the SGF/SEBS/PP hybrid (route 2) tested at an impact velocity of 3 m s^{-1} were relatively clean. The main features of the fractograph were fiber debonding and pullout [Fig. 9(b)].

Dynamic mechanical behavior

DMA can provide information on possible shifts in the glass-transition temperatures (T_g's) of the SEBS and PP phases of these hybrids. Figure 10(a) shows the loss tangent (tan δ) versus the temperature for the hybrids

TABLE III
Transition Temperatures of the EB Segment of SEBS (T_{g1}) and the PP Phase (T_{g2}) of the Hybrids

Sample	T_{g1} (°C)	T_{g2} (°C)
SGF/SEBS/PP (route 1)	−41.7	16.6
SGF/SEBS/PP (route 2)	−40.2	15.7
SGF/SEBS-*g*-MA/PP (route 1)	−36.4	15.9
SGF/SEBS-*g*-MA/PP (route 2)	−38.3	16.3

investigated. The tan δ curves of the hybrids exhibit two relaxations located around −40 and 16°C. McCrum et al.[13] reported that tan δ of pure PP showed three relaxations at −80 (γ), 8 (β), and 100°C (α). The γ peak was thought to be associated with the relaxation of small chain groups such as methyl and methylene. The dominant β relaxation was assigned to T_g. The small α relaxation could be attributed to a lamellar slip mechanism.[13] Ghosh et al.[14] indicated that the SEBS block copolymer displays three relaxation peaks at −105 (γ), −36 (β), and 109°C (α). The α transition was due to the relaxation of the hard polystyrene segment, the β dispersion was due to the relaxation of the soft poly(ethylene butylene) segment, and the γ transition was associated with the crankshaft movement of the $(—CH_2—)_n$ units present in the poly(ethylene butylene) segment.[14] In this aspect, the relaxation peak of the hybrids investigated at approximately −40°C corresponded to T_g of the EB midblock of SEBS, whereas the peak at approximately 16°C was associated with T_g of PP. The results are listed in Table III. It is apparent that the addition of MA functional groups to SEBS shifted T_g of SEBS toward that of PP. The α relaxation of PP overlapped with the α relaxation of the styrene domain of the SEBS copolymer, and this transition did not appear in the tan δ spectrum. Figure 10(b) shows the variation of the loss modulus with the temperature for the hybrids studied. The α relaxation of the hybrids was easier to observe in the loss modulus curves and appeared as a broad and flat shoulder in the spectrum of the SGF/SEBS/PP hybrid prepared by route 1. The loss modulus was related to the dissipation of energy as heat due to the deformation of the materials. It provided information about the transformation of change in the materials as a function of temperature. From Figure 10(b), it seems that the lamellar movement in the crystalline phase of PP was affected by SGF and MA functional groups. The α relaxation became sharper and appeared as a hump peak for the SGF/SEBS-*g*-MA/PP hybrid. Its maximum shifted toward a lower temperature of approximately 73°C.

CONCLUSIONS

This work was an attempt to study the process–structure–property relationship of the SGF/SEBS/PP and SGF/SEBS-*g*-MA/PP hybrids. The results showed that route 2 (or the sequential blending process) promoted a finer dispersion of SEBS elastomers in the SGF/SEBS/PP and SGF/SEBS-*g*-MA/PP hybrids. An SEBS elastomeric interlayer tended to form more uniformly at the SGF and matrix interface of the SGF/SEBS-*g*-MA/PP hybrid (route 2). This SEBS rubbery layer enhanced the interfacial bonding between the SGF and matrix of the SGF/SEBS-*g*-MA/PP hybrid (route 2). It promoted efficient stress transfer across the fiber–matrix interface during tensile tests and relieved the triaxial stress imposed by the plane strain constraint at the notch tip during impact loading. Therefore, it triggered extensive plastic deformation in the matrix region adjacent to the fiber ends during impact tests. Consequently, the SGF/SEBS-*g*-MA/PP hybrid (route 2) exhibited the highest modulus, yield stress, tensile stress at break, Izod impact energy, and Charpy drop weight impact strength among the composites investigated.

References

1. Gupta, A. K.; Purwar, S. J. J Appl Polym Sci 1986, 31, 535.
2. Bassani, A.; Pessan, L. A.; Hage, E. J Appl Polym Sci 2001, 82, 2185.
3. Setz, S.; Stricker, F.; Kressler, J.; Duscher, T.; Mulhaupt, R. J Appl Polym Sci 1996, 59, 1117.
4. Stricker, F.; Mulhaupt, R. J Appl Polym Sci 1996, 62, 1799.
5. Stricker, F.; Friedrich, K.; Mulhapt, R. J Appl Polym Sci 1998, 69, 2499.
6. Jancar, J. J Mater Sci 1996, 31, 3983.
7. Tam, W. J.; Cheung, T. Y.; Li, R. K. Y. J Mater Sci 2000, 35, 1525.
8. Wu, J.; Yu, D.; Chan, C. M.; Kim, J.; Mai, Y. W. J Appl Polym Sci 2000, 76, 1000.
9. Friedrich, K. J Mater Sci 1998, 33, 5535
10. Mohd Ishak, Z. A.; Ishiaku, U.; Karger-Kocsis, J. J Mater Sci 1998, 33, 3377.
11. Tjong, S. C.; Xu, S. A.; Li, R. K. Y.; Mai, Y. W. J Appl Polym Sci 2002, 86, 1303.
12. Mouzakis, D. E.; Stricker, F.; Mulhaupt, R.; Karger-Kocsis, J. J Mater Sci 1998, 33, 2551.
13. McCrum, N.; Read, B.; William, G. Anelastic and Dielectric Effects in Polymer Solids; Wiley: London, 1967.
14. Ghosh, S.; Bhowmick, A. K.; Roychowdhury, N.; Holden, G. J Appl Polym Sci 2000, 77, 1621.